

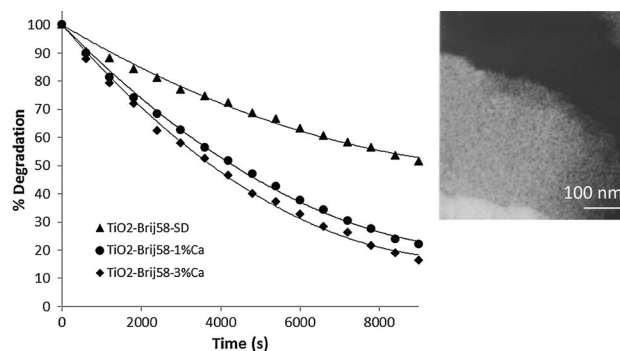
Ca doping of mesoporous TiO₂ films for enhanced photocatalytic efficiency under solar irradiation

Y. Castro¹ · A. Durán¹

Received: 24 November 2015 / Accepted: 18 February 2016 / Published online: 3 March 2016
© Springer Science+Business Media New York 2016

Abstract Anatase mesoporous TiO₂ films doped with Ca were prepared by sol–gel and deposited onto glass slides. The influence of the dopant in the textural and structural properties of the films was studied together with their photocatalytic activity. Titania sols w/o and with Ca were synthesised from titanium isopropoxide as TiO₂ precursor, acetic acid as complexing agent, and polyethylene glycol hexadecyl ether (Brij58) as pore-generating agent. The TiO₂ films were characterised by Fourier transform infrared spectroscopy, Raman spectroscopy, and transmission electron microscopy. Environmental ellipsometric porosimetry was used to obtain the adsorption–desorption isotherms and the total pore volume, for determining the pore size distribution and specific surface area (S_s) of the films, crucial parameters that govern the photocatalytic behaviour. The photocatalytic activity was evaluated through the degradation of methyl orange (MO) in aqueous solution using a Xe lamp that simulates solar radiation. The photocatalytic activity depends on the dopant amount. The dopant creates levels within the band gap that improving the charge separation, and reduces the recombination e^-/h^+ pairs. The best results of MO degradation were obtained for the films sintered at 450 °C for 90 min and doped with 3 % of Ca²⁺.

Graphical Abstract



Keywords Mesoporous TiO₂ films · Sol–gel coatings · Dopants · Photocatalysis · Degradation of methyl orange (MO) · Solar irradiation

1 Introduction

Titanium dioxide (TiO₂) is considered a good semiconductor because of its exceptional optical and electronic properties, strong oxidising power, non-toxicity, easily available, low cost, and long-term stability against photo-corrosion and chemical corrosion, along with its high photocatalytic efficiency. The most important application of TiO₂ is related with the degradation of pollutants in water and gas phase by advanced oxidation processes, together with bactericidal applications when TiO₂ is doped with silver nanoparticles [1–4]. In the industrial sector, the use of TiO₂ particles is not always feasible due to the high costs of the filtration facilities needed to recover the catalyst after use. Therefore, processes focused on supported

✉ Y. Castro
castro@icv.csic.es

¹ Instituto de Cerámica y Vidrio (CSIC), Campus de Cantoblanco, 28049 Madrid, Spain

catalysts with high catalytic performance are considered. Deposition of TiO₂ films on transparent substrates is a suitable procedure to immobilise the photocatalyst avoiding the release of nanoparticles into the medium [5, 6].

A large variety of methods have been developed to prepare TiO₂ films, but sol–gel is one of the most widely used since it permits obtaining coatings at much lower temperatures than conventional processing. The use of templates allows the self-assembly of organised micelles and creates mesoporous films with high specific surface area. The textural and morphological properties greatly affect the photocatalytic properties. Different studies indicate that photocatalytic activity mainly depends on the total surface effectively irradiated with UV photons [7, 8] and on the size of the pores [9].

A disadvantage of using TiO₂ with solar illumination resides in its bandwidth; the radiation absorption threshold is around 380 nm (3.2 eV), this means that titania takes very little advantage of the solar spectrum; only between 4 and 6 % of the total intensity of sunlight [10] can photoactivate to produce charge carriers. Considering that the reaction rate of the photocatalytic process is proportional to irradiation, this is a significant limitation. Thus, it is important to look for routes to shift the optical gap towards lower energy or extend the wavelength range absorption of TiO₂ into the visible region. On the other side, the increasingly stringent regulations open up opportunities for novel green photocatalytic routes leading to the substitution or modification of TiO₂, an ultraviolet (UV) absorber, in order to allow the use of sunlight (UV–Vis light) as the energy source for fine chemical production processes. The goal was to produce enhanced photocatalysts adapted to the solar spectrum by developing new semiconductors or modifying the TiO₂ by doping with transition metals, cations, or anions to arrive to better performances. Different reports [11, 12] showed that the production of metal-doped TiO₂ can enhance photoinduced surface redox reactions even in visible light region.

The efficiency of a dopant depends on different parameters such as its concentration and distribution in TiO₂ matrix, the creation of additional energy levels in the band gap, and the electron donor concentration. For example, an excess of dopant concentration could produce a detrimental effect decreasing the photocatalytic activity, because the charge recombination is favoured [13].

The doping of TiO₂ with noble metals, such as Au, Ir, Os, Rh, Ru, Pt, and Pd, generates structural changes in the coatings, like smaller TiO₂ crystal size and changes in the interplane distances of the crystalline network. Their main effect is usually to increase the acceptance capacity of photogenerated electrons, preventing the recombination processes and, at the same time, enhancing the reduction processes on the metal surface [14]. However, the energy level and d-electron configuration of the dopants are

critical factors to consider in the process of generating electron–hole pairs in TiO₂.

The most popular transition metals used as dopants are W, V, Cr, Fe, Co, Mn, and Cu which modify the optical and photoelectrochemical properties of TiO₂, shifting the light absorption of TiO₂ to the visible region and prolonging the lifetime of electron and holes, thus increasing the photocatalytic activity [15–17]. The principal effect of these dopants is to create additional intermediate energy levels that modify the electrical and optical properties of the TiO₂ matrix and inhibit the recombination of photoinduced e^-/h^+ pairs and shifts the TiO₂ band gap. Iketani [18] highlighted the importance of the oxidation state of V; V⁵⁺ reduces the photocatalytic activity as compared to the high photocatalytic efficiency of V⁴⁺. In other cases, the increment of dopant content favours the crystallisation of rutile phase [19], and the photocatalytic activity decreases.

On the other hand, the photocatalytic properties of TiO₂ are modified when doped with alkaline and alkaline earth ions. Al-Salim et al. [20] considered that the photocatalytic activity of TiO₂ films doped with Ca²⁺ increases because Ca²⁺ ions could create oxygen vacancies or interstitial substitutions. The development of oxygen vacancies by metal ion doping leads to new phase formation, which acts as a sensitiser. The size distribution of such sensitiser in the TiO₂ matrix plays a significant role in visible light degradation.

Many studies have demonstrated the effectiveness of Ca²⁺ dopant for enhancing the photocatalytic activity of TiO₂ under UV radiation or visible light [12, 21, 22], but a few reports analyse the properties under solar irradiation [23]. Furthermore, it is difficult to obtain definite conclusions on the effects of Ca doping on the photoactivity.

The aim of this work was to explore the potential of using Ca²⁺, with valence lower than Ti⁴⁺, for doping TiO₂ to improve its visible photocatalytic activity. Mesoporous nanocrystalline TiO₂-anatase films doped with Ca²⁺ were prepared using Brij58 as surfactant. The photocatalytic activity of Ca–TiO₂ films was studied by varying the Ca amount and the heat treatment of the coatings. The different parameters ruling the photoactivity, such as film thickness, crystallinity, total pore volume, specific surface area, and total surface exposed to illumination, were considered, along with the analysis of the textural properties that allow advancing in the relationship between photocatalytic properties and film structure.

2 Experimental section

2.1 Synthesis and characterisation of undoped and Ca-doped TiO₂ sols

Ca-doped TiO₂ sols were prepared using titanium isopropoxide (TISP, Aldrich, 284.22 g/mol, 97 %) as

precursor via acid catalysis. TISP was chemically modified by mixing with acetic acid (AcOH, Aldrich, 60.05 g/mol, 99.99 %) and absolute ethanol, in order to control the hydrolysis and condensation reactions. After 1 h of stirring, polyethylene glycol hexadecyl ether P5884 (Brij58, Aldrich, 1124 g/mol) was added to the solution TISP/EtOH/AcOH. Then, $\text{Ca}(\text{NO}_3)_2$ (Aldrich, 236.15 g/mol, 99 %) was incorporated using different molar ratios $\text{Ca}(\text{NO}_3)_2/\text{TISP} = 0.01$ and 0.03. Finally, a mixture of ethanol and acidified water (0.1 M HCl) was added drop by drop onto the solutions, up to a final oxide concentration of 30 g/L.

The final molar ratio was fixed to 1 TISP:1 AcOH:40 EtOH:0.07 Brij58:2 H_2O :(0.01–0.03) Ca. All the sols were aged for 2 days before coating deposition.

Two reference sols were prepared: TiO_2 –Brij58–SD sol was obtained following the same process without the addition of Ca and TiO_2 –SD sol without Ca and Brij58.

The stability of the sols was studied through the evolution of viscosity with time, using an Ostwald viscometer (Pobel, 0c model, viscosity range 0.6–3 mPas).

2.2 Deposition of undoped and Ca-doped TiO_2 films

Undoped and doped TiO_2 thin films were deposited by dip-coating combined with evaporation-induced self-assembly (EISA) method onto glass slides and silicon wafers. The films were obtained at 35 cm/min and 20 % relative humidity (RH), and heat-treated in air at 450 °C for 60 or 90 min using a heating ramp of 10 °C/min. In the case of multilayer coatings, the same withdrawal rate was used along with an intermediate heat treatment of 350 °C/1 h between coatings followed by a final treatment of 450 °C for 60 or 90 min.

The glass slides used to measure the photocatalytic activity were coated with a first layer of SiO_2 , using a SiO_2 sol prepared in two steps using TEOS (tetraethoxysilane). SiO_2 coatings were sintered at 450 °C for 30 min, obtaining a thickness of ~ 210 nm, and a refractive index of ~ 1.44 , corresponding to 98 % of theoretical density of SiO_2 . The quite dense SiO_2 coating avoids the diffusion of Na^+ cations from the glass substrate to the TiO_2 coating during firing and the possible inhibition of photocatalytic activity [24, 25].

2.3 Characterisation of doped films

The coatings were characterised by optical microscopy (Zeiss, HP1, Germany) to detect the presence of precipitates, impurities, bubbles, or cracks, and studied by transmission electronic microscopy (TEM) (Hitachi H-7100, Japan) to confirm the homogeneity and porous structure of

the films. TEM samples were obtained by scratching the films and depositing the scaled fragments onto carbon-coated copper grids.

Ellipsometry and environmental ellipsometric porosimetry (EEP) measurements were taken using a spectral Ellipsometer (M-2000UTM, J.A. Co., Woollam) modified with a system that allows controlling the relative humidity (RH) (Humidity Generator HG-1, Michel Instruments) to characterise films deposited onto glass slides. The spectra were taken between 250 and 900 nm at a fixed incident angle of 70°. The data were fitted using the WVASE32 software with a Cauchy model. From the fitting data, the refractive index (n) (taken at $\lambda = 700$ nm) and the thickness (e) of the films were obtained as a function of relative humidity RH (from 0 % to 100 %). The total pore volume and the adsorption–desorption isotherms were further obtained by considering the Bruggeman effective medium approximation model (BEMA) and a reference TiO_2 coating obtained using the TiO_2 –SD sol. The pore size distributions were calculated utilising a modified Kelvin equation taking into account ellipsoidal pore geometry [26]. Finally, specific surface area and exposed surface area per cm^2 of sample were calculated [9].

The hydrophobic–hydrophilic character of the coatings was evaluated through the variation in the contact angle using an Easy Drop equipment (“Drop Shape Analysis System” Kruss DSA 100).

Raman spectra were measured in back-scattering using a confocal Raman microscope (Witec alpha-300R). The samples were excited with 514.5-nm line of an Ar^+ ion laser.

The crystallisation behaviour was followed by grazing incidence X-ray diffraction (GIXRD) of undoped and doped TiO_2 coatings deposited on Si wafers. GI-XRD spectra were obtained using synchrotron radiation with a wavelength of $\lambda = 0.62$ Å in the BM25B Spanish Line (SpLine), at the European Synchrotron Radiation Facility (ESRF, Grenoble, France). The 2θ scanning angle was varied between 8° and 25° with a step of 0.034°, a counting time of about 5 s, and varying the grazing angle between 0.08° and 0.15°.

UV–Vis absorption spectra of TiO_2 layers deposited on quartz glass were recorded using a Lambda 950 spectrophotometer (PerkinElmer Inc., USA) equipment in the range of 200–2000 nm. The band gap was determined using the Eq. (1).

$$(\alpha E)^{1/m} = A (E - E_g) \quad (1)$$

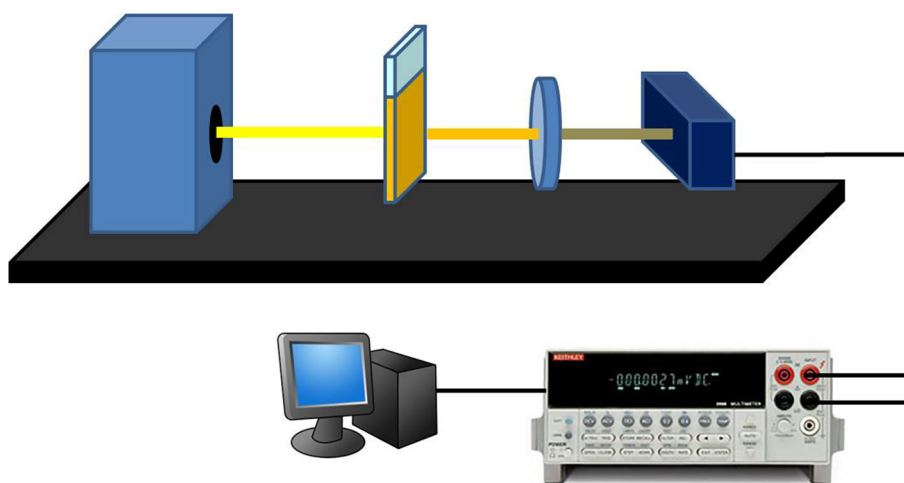
where α is the absorption coefficient, E_g is the band gap energy, E is the energy of the incident photon, A is a constant, and m is a parameter that depends on the electronic transition of the semiconductor; for indirect transition semiconductor such as TiO_2 -anatase phase, $m = 2$ [4, 27].

The photocatalytic activity was evaluated by the degradation of methyl orange (MO) [28, 29] in aqueous solution using the films deposited onto glass slides on top of a first layer of SiO_2 . The light source (Oriel, model 96000) is equipped with a solar light simulating Xe-arc lamp (Osram XBO 450 W) with commercial AM 6197 filter.

The tests were performed using 25 mL of aqueous solution of methyl orange (MO) with a concentration of $c = 3 \text{ mg/L}$. The pH of the solution was adjusted to 2 using HCl [30], and the total surface tested was equal to 25 cm^2 . The quartz reactor vessel is covered with window glass to prevent solution evaporation. First, photolysis and dark tests (adsorption) were performed to confirm that the degradation of MO is only associated with the TiO_2 film and not to light irradiation and/or adsorption.

Photocatalytic measurements were taken introducing the TiO_2 samples in the MO solution and maintained under continuous stirring and irradiation. The degradation was monitored using a home-made system depicted in Fig. 1. Beyond the sample, a narrow bandpass filter with centre at 500 nm and bandwidth of 10 nm (Thorlabs, FB-500-10 full width at half maximum) was placed in front of a biased Silicon Photodetector (Thorlabs DET100A). The filter limits allow the light transmission in a wavelength range that matches the absorption band of the MO (508 nm). Therefore, the intensity of light at the detector allows measuring the degradation of MO. All the elements were mounted on an optical table to ensure stability and optically isolated in the dark to avoid the presence of other light sources. The output signal from the detector (voltage) was sent to a Keithley 2010 multimeter. The signal at the multimeter was recorded every 10 min with a PC computer using a Visual Basic home-made code.

Fig. 1 Device to monitor the degradation of MO



3 Results and Discussion

3.1 Characterisation of doped TiO_2 sols and structure of the films

The stability of undoped and doped TiO_2 sols was evaluated following the evolution of viscosity with ageing time at $25 \text{ }^\circ\text{C}$. In all the cases, a Newtonian behaviour was observed with initial viscosities between 1.5 and 2 mPa s , without significant change for at least 1 month, thus revealing an excellent stability. The doping does not affect the stability of TiO_2 sols.

Multilayer TiO_2 films deposited onto glass slides from undoped and doped TiO_2 -Brij58 sols were characterised by Raman spectroscopy. Figure 2 shows the Raman spectra of undoped and Ca-doped mesoporous TiO_2 -Brij58-Ca films treated at $450 \text{ }^\circ\text{C}$ for 60 min. The bands observed in Fig. 2 reveal the presence of anatase phase with tetragonal structure that corresponds to the space group D_{4h}^{19} (I4/amd) [31, 32]. The Raman-active modes are clearly distinguishable, indicating the crystallisation of anatase phase without the presence of brookite and rutile phases. However, the dopant concentration and the heat treatment time affect the intensity and broadness of the peaks and therefore the structure (crystal size and crystalline fraction) [33]. In order to evaluate the differences among samples, the position and the full width at half maximum [FWHM] of the E_g mode at 144 cm^{-1} were established (Table 1). A slight shifting of the bands to lower frequencies is observed suggesting an alteration in the crystal symmetry and/or a lattice distortion, originating a non-stoichiometric material that affects the photocatalytic activity. On the other hand, the FWHM increases for 1 % mol of Ca^{2+} , but decreases again for 3 % mol Ca^{2+} , indicating small changes in the crystal size. In general, the change in width and shift of the Raman bands is associated with the presence of impurity

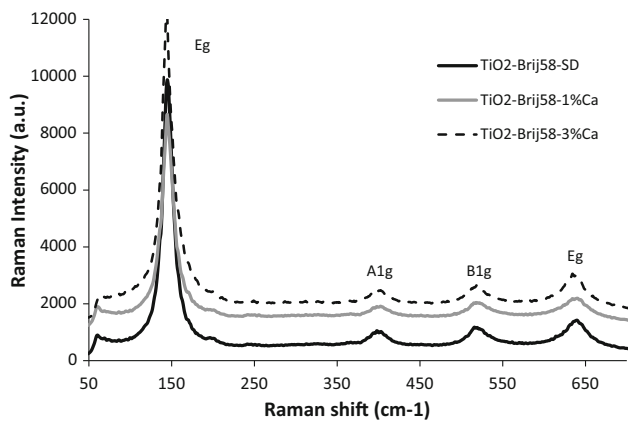


Fig. 2 Raman spectroscopy spectra of doped and undoped mesoporous TiO₂ films heat-treated at 450 °C for 60 min

Table 1 Position of E_g Raman-active mode and FWHM for TiO₂ anatase

Sample	Position of the E_g mode (cm ⁻¹)	FWHM (cm ⁻¹)
TiO ₂ -AcOH-Brij58; 60 min		
Undoped	145.25	16.11
1 % Ca	145.10	16.61
3 % Ca	144.69	16.02
TiO ₂ -AcOH-Brij58; 90 min		
Undoped	145.07	14.62
1 % Ca	144.93	15.20
3 % Ca	144.67	14.80

atoms, as well as with the number of defects. In this case, the introduction of Ca²⁺ as an impurity in the TiO₂ network could explain the different intensity and broadness of the peaks between undoped and doped coatings and explain the photocatalytic behaviour.

Crystal size was obtained by GIXRD as a function of dopant and sintering time for coatings deposited onto Si wafer. Figure 3 shows the diffraction patterns of TiO₂-Brij58-Ca film treated at 450 °C/90 min, where anatase was identified as the only crystalline phase present, confirming the Raman studies. Peaks associated with the Si wafer substrates were observed and identified. The crystal size was calculated using the Scherrer's equation and considering the peaks of anatase (101) and (004) (Fig. 3). For undoped TiO₂ films, the average crystal size increases with the sintering time, going from 8.9 to 9.8 nm for TiO₂-SD-60 min and TiO₂-SD-90 min, respectively. The incorporation of Ca²⁺ slightly increases the crystal size (Table 2) with respect to undoped coatings, but this size does not significantly change with the sintering time. The position of (101) peak of anatase was estimated using GIXRD spectrum and is shown in Table 2. The (101) peak

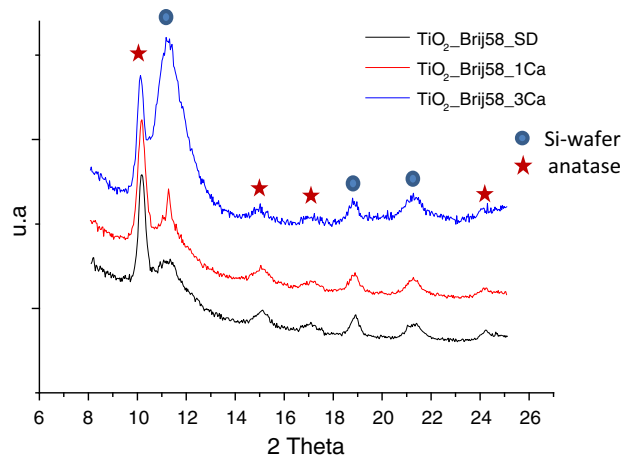


Fig. 3 GIRDX measurement of TiO₂-Brij58-Ca films heat-treated at 450 °C/90 min

Table 2 Crystal size for doped and undoped TiO₂ films heat-treated at 450 °C

Composition	Position of peak (101)	Crystal size (nm) ± 0.3
TiO ₂ -AcOH-Brij58; 60 min		
Undoped	10.126	8.9
1 % Ca	10.073	10.2
3 % Ca	10.050	10.9
TiO ₂ -AcOH-Brij58; 90 min		
Undoped	10.192	9.8
1 % Ca	10.179	9.9
3 % Ca	10.122	10.9

is shifted to lower angles for Ca-doped TiO₂ films compared to TiO₂ films, this shift increases with the increment of Ca²⁺. Some reports associate this displacement with the insertion of Ca²⁺ cation within the anatase matrix [21]. This inclusion produces the distortion of TiO₂ lattice as observed by Raman and would be advantageous for the photocatalytic activity.

The lattice parameters for TiO₂-Brij58-SD and TiO₂-Brij58-3%Ca 60-min samples were determined considering a tetrahedral crystal structure and a single anatase phase (Table 3). The lattice parameter “a” decreases in the doped sample respecting to undoped coating, whereas the parameter “c” increases, indicating a deformation of TiO₂ tetrahedra. This deformation could be related with the incorporation of Ca²⁺ ions in interstitial sites in de TiO₂ network [12, 22] and with the generation of defects.

The band gap (E_g) of Ca-doped TiO₂ films was determined from UV-Vis spectral data and using the Eq. 1. For TiO₂-Brij58-SD and TiO₂-Brij58-Ca samples, values of 3.64 and 3.7 eV were obtained. Considering an error of 0.05 eV, the E_g maintains near constant, and the introduction of Ca²⁺ did not affect the final values.

Table 3 Lattice parameters for undoped and 3 % Ca–TiO₂–Brij58 films heat-treated at 450 °C/60 min

Composition	Lattice parameters (Å)	
	<i>a</i> (±0.0025)	<i>c</i> (±0.0025)
TiO ₂ –Brij58 60 min	3.787	9.437
TiO ₂ –Brij58–Ca 60 min	3.768	9.472

These results indicate that the introduction of Ca²⁺ in TiO₂-anatase films does not greatly affect the structure of the coatings. The crystal size remains unchanged, as the band gap. Only slight changes in the symmetry of the crystals are appreciated, likely originated by distortions of the lattice produced by defects associated with Ca²⁺.

3.2 Textural characterisation of TiO₂ films

Spectral ellipsometry and environmental ellipsometric porosimetry (EEP) permit to characterise properties such as optical constant, thickness, refractive index, and porosity properties of the films. Cauchy model for transparent films was used to obtain thickness and refractive index.

The textural properties are summarised for doped and Ca-doped TiO₂ films in Table 4 together with the contact angle.

The thickness (*e*) and refractive index (*n*) of the coatings were measured as a function of sintering conditions and dopant amount. Increasing the sintering time does not significantly change *e* and *n*. The refractive index varies between 1.67 and 1.73 and the thickness between 308 and 335 nm. Thus, Ca doping of the coating does not substantially change the optical parameters.

On the other hand, the total pore volume fraction (*V*_{pore}) was calculated by Bruggeman effective medium approximation (BEMA) model. All the coatings presented high *V*_{pore} around 30–35 %. The pore size distribution was calculated through the variation in the refractive index and

thickness with the relative humidity and using the modified Kelvin’s equation.

Figure 4a, b shows the water adsorption–desorption isotherms and the pore size distribution for TiO₂–Brij58–1%Ca 60-min film respectively. A reversible type IV adsorption–desorption isotherm with hysteresis loop is observed (Fig. 4a), indicating the presence of pores in the mesoporous range (2–50 nm). TiO₂–Brij58–1%Ca 60-min film presents a total pore volume of 35 % (Fig. 4a) and a pore size of 6.1 nm (Fig. 4b). The rest of the samples exhibit isotherms with similar shapes (not shown).

All the films presented pore sizes between 4.7 and 6.1 nm (Table 4), the increment of Ca dopant slightly increasing the pore size; however, when the sintering time increases, the pore size remains near constant (~ 6 nm). Longer sintering times could stabilise the network of TiO₂ avoiding the deformation or collapse of the pores.

The specific surface area (*S*_s) and the exposed area (*S*_{exp}) were also calculated [26] (Table 4). This last parameter represents the total area exposed to irradiation, thus being relevant for photocatalytic behaviour. All the coatings present *S*_s and *S*_{exp} between 200–233 m²/cm³ and 60–75 cm².

Finally, the Ca-doped TiO₂ films present significantly lower contact angles (*θ*) with respect to undoped coatings (~ 25°), showing that dopant increases the hydrophilicity of the films; this behaviour agrees with the results reported by Yuan et al. [34] and is significant for the photocatalytic properties since it improves the contact between the pollutant containing solution and the material, facilitating the catalytic reactions.

Transmission electronic microscopy (TEM) confirmed the porous structure of the coatings. Figure 5 shows the micrographs of TiO₂–Brij58–SD and TiO₂–Brij58–Ca films. All the films present similar mesoporous structures in agreement with the porosity characterisation obtained by EEP. The mesoporosity is homogeneously distributed not presenting a defined order.

Table 4 EEP characterisation for doped and undoped TiO₂ films heat-treated at 450 °C for 60 and 90 min

Composition	<i>e</i> (nm) ± 0,02	<i>n</i> ± 0.05	<i>V</i> _{pore} (%) ± 5 %	<i>φ</i> (nm) ± 10 %	<i>S</i> _s (m ² /cm ³) ± 10 %	<i>S</i> _{exp} (cm ²) ± 10 %	<i>θ</i> (°)
60 min							
Undoped	331	1.73	29.7	4.7	227	68	27
1 % Ca	308	1.69	35.1	6.1	214	70	9.9
3 % Ca	310	1.74	32.1	5.8	218	70	9.5
90 min							
Undoped	335	1.66	34.0	5.7	212	71	25
1 % Ca	315	1.70	35.0	6.1	210	71	15.5
3 % Ca	318	1.69	34.9	6.2	215	68	10.1

Fig. 4 Adsorption–desorption isotherm (a) and pore size distribution (b) for TiO₂–Brij58–1 %Ca 60-min film

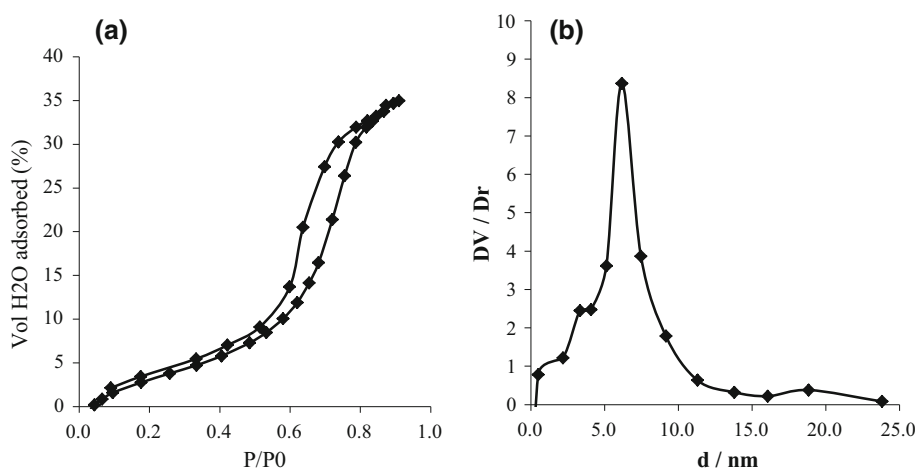
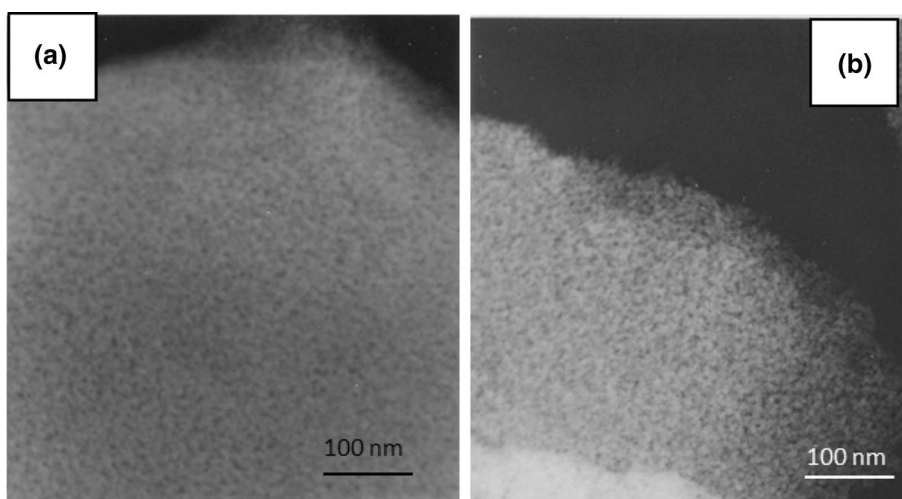


Fig. 5 TEM micrographs of undoped films —TiO₂–Brij58 (a) and TiO₂–Brij58–1%Ca 60 min (b)



The results included in Table 4 indicate that Ca doping of titania-anatase mesoporous films does not significantly affect their optical properties (n and e) and texture. Similar pore volume, pore size, S_s , and S_{exp} were obtained for doped films. The only parameter with a significant change was the contact angle that clearly decreases for doped samples.

3.3 Photocatalytic activity of TiO₂ films

The photocatalytic activity of undoped and doped TiO₂ films was evaluated through the degradation of methyl orange (MO) [9]. The preliminary tests showed that neither photolysis nor adsorption processes occur.

Figures 6 and 7 present the photocatalytic behaviour of undoped and Ca-doped TiO₂–Brij58 films sintered at 450 °C for 60 and 90 min.

The photocatalytic efficiency of TiO₂ films is clearly enhanced by the incorporation of Ca²⁺ doping, the final

performance depending on Ca content and sintering time. TiO₂–Brij58–1%Ca sintered for 60 min and TiO₂–Brij58–3%Ca treated during 90-min films showed decomposing rates of 79 and 83 % of MO after 2.5 h under solar irradiation, respectively (Figs. 6, 7), corresponding with the highest degradation performance. Undoped TiO₂–Brij58 films present the lower degradation rate (37 %) compared to Ca-doped TiO₂ films in both sintering conditions (79–83 %, respectively).

For obtaining the kinetic parameters, the photocatalytic decomposition of MO was described by a first-order kinetic model [35], $-\ln(C_0/C) = kt$, where C_0 and C are the concentrations at $t = 0$ and at time t . The plots of $\ln(C_0/C)$ versus t show a straight line with a slope k that is the apparent first-order reaction constant (Fig. 8). On the other hand, heterogeneous catalysis is a surface phenomenon, so it is well known that the overall kinetic parameters are dependent from the real (exposed) surface of the active semiconductors. A possible approach to the photocatalytic

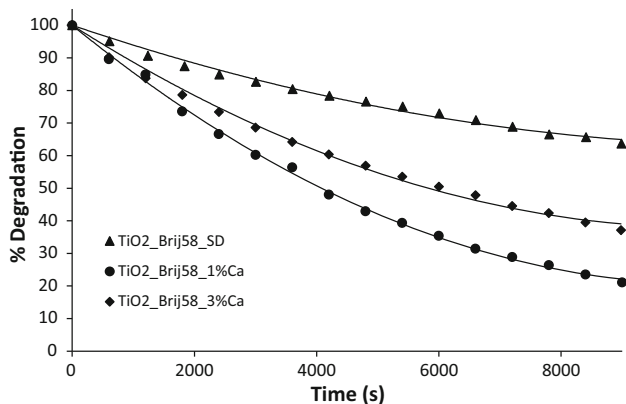


Fig. 6 Photocatalytic degradation of methyl orange ($c = 3 \text{ mg/L}$) for doped and undoped TiO_2 -Brij58 films heat-treated at $450 \text{ }^\circ\text{C}/60 \text{ min}$

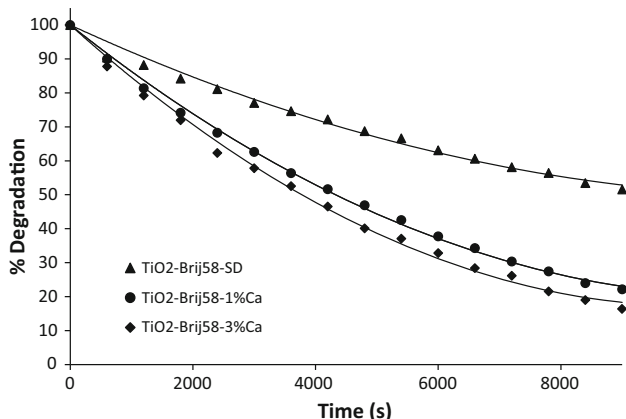


Fig. 7 Photocatalytic degradation of methyl orange ($c = 3 \text{ mg/L}$) for doped and undoped TiO_2 -Brij58 films heat-treated at $450 \text{ }^\circ\text{C}/90 \text{ min}$

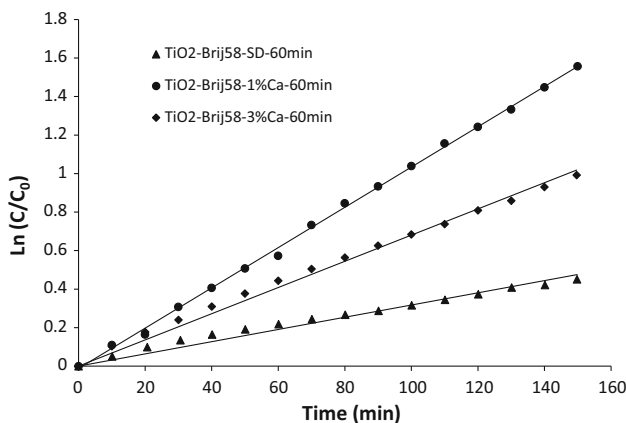


Fig. 8 First-order kinetics for Ca-doped and undoped TiO_2 -Brij58 films sintered at $450 \text{ }^\circ\text{C}$ for 60 min

efficiency is described for a new kinetic parameter, K' , which would express the degradation efficiency per unit area of the catalyst, defined as $K' = k/(S_{\text{exp}})$ [36]. Table 5 shows the first-order rate constants, k , together with the

Table 5 Kinetic constants and lifetime for all the TiO_2 coatings heat-treated at $450 \text{ }^\circ\text{C}$

Composition	k (k/min)	K' (k/ S_{exp})	$t_{1/2}$ (min)
60 min			
Undoped	0.0031	4.5×10^{-5}	223
1 % Ca	0.0105	1.5×10^{-4}	66
3 % Ca	0.0068	9.4×10^{-5}	101
90 min			
Undoped	0.0046	6.4×10^{-5}	150
1 % Ca	0.0100	1.5×10^{-4}	69
3 % Ca	0.0118	1.8×10^{-4}	58

normalised rate constants, K' , and the $t_{1/2}$ (the time at which the remaining concentration of MO is half of the initial concentration) for the different TiO_2 films used in this study.

The k value parameter of TiO_2 -Brij58-3%Ca 90-min film was 0.0118 min^{-1} , the highest value among all the photocatalysts considered and associated with a $t_{1/2}$ of 58 min. This photocatalyst has specific reactive sites that act as efficient traps favouring the formation of reactive hydroxyl radicals. Ca-doped TiO_2 films show a stronger effective degradation rate together with TiO_2 -Brij58-1%Ca 60-min (0.0105 min^{-1}) film. Undoped TiO_2 films present the lowest efficiency, with $t_{1/2}$ of 223 and 150 min.

The differences in the reaction rates are usually due to morphological and/or structural changes induced by the incorporation of a dopant. But new arguments should be taken into account because these changes are not relevant in Ca-doped titania films obtained in this study as described in previous sections.

Indeed, to explain the photocatalytic behaviour, two main aspects have to be considered: one associated with the structural, textural, and porous structure of the coatings, and other related with the nature of the dopant and the effect in the electronic structure of titania-anatase. One main objective of doping was to induce a change in spectral band position that results in the increased absorption of visible light. This change could be induced by (1) a decrease in the band gap or (2) a modification of intra-band gap states, both changing the electronic structure of TiO_2 .

In this case, the band gap is not affected by the incorporation of Ca^{2+} and it cannot explain the enhanced photocatalytic behaviour of doped samples.

With respect to the textural properties (Table 4), TiO_2 -Brij58-Ca 90-min films present a pore size $\sim 6.0 \text{ nm}$ associated with a high specific exposed surface area ($S_s \sim 70 \text{ cm}^2$). Chen and Dionysiou [37] demonstrated that the photocatalytic activity depends on the pore size photocatalysts with pore size around 5 nm being the most

adequate to obtain high degradation rates. However, all the studied coatings present a similar structure (pore size, S_s and S_{exp}). Therefore, these parameters are neither determinant to explain the better performance of doped photocatalysts. Only the contact angle is significantly lower for Ca–TiO₂ coatings, which could explain a larger wettability and an increase in the photocatalytic activity.

So, the most probable origin of the enhanced photocatalytic activity should be related with the intercalation of Ca²⁺ cation into the TiO₂ network and the modification of electronic states within the band gap. Different authors report that Ca²⁺ could be isomorphously substituted or interstitially introduced into the matrix inducing oxygen vacants or interstitial Ti³⁺ ions [21, 22]. Both effects can increase the photocatalytic activity. However, considering that the radius of Ca²⁺ (0.99 Å) is much bigger than that of Ti⁴⁺ (0.68 Å) and closer to O²⁻ (1.26 Å) [38], the more probable situation according to Raman and GIXRD results points to the location of Ca²⁺ in interstitial sites in TiO₂-anatase crystals, thus producing a lattice deformation and/or generating defects in the semiconductor structure. Impurity bands are likely created within the band gap that will increase the photocatalytic activity. These defects might improve the charge separation and reduce the recombination e^-/h^+ pairs, acting as bridge for electron transitions, likely explaining the enhanced photocatalytic activity of photocatalyst doped with Ca [39].

The much enhanced efficiency of Ca²⁺-doped mesoporous titania films converts these materials into suitable and cost-effective candidates for indoor and outdoor applications.

4 Conclusions

The incorporation of Ca²⁺ ions in the network of TiO₂ films prepared by sol–gel greatly increase the photocatalytic degradation of methyl orange (MO) and its kinetic when measured under simulated solar irradiation Xe lamp.

The incorporation of Ca²⁺ in the TiO₂ network modifies the unit cell, as observed by Raman and GIXRD.

The highest efficiency was found for the films TiO₂–Brij58–1%Ca sintered for 60 min and TiO₂–Brij58–3%Ca treated during 90 min. Neither the band gap measurements nor the structural and textural properties change appreciably with the Ca doping of the coating; therefore, they cannot explain the differences in the photocatalytic activity.

The substitution of Ti⁴⁺ ions by Ca²⁺ in the TiO₂ matrix likely modifies the impurity level of electronic bands increasing the stabilisation of the anatase phase.

The introduction of Ca²⁺ ions in interstitial positions of Ti⁴⁺ in the TiO₂ matrix likely contributes to enhance the photocatalytic activity.

Acknowledgments This work was supported by PIE-CSIC-2004-60E637. The authors acknowledge Aritz Iglesias for the experimental work and Adolfo del Campo for the Raman measurements. The authors also thank German Castro and Juan Rubio of Spanish CRG BM25-SpLine at the European Synchrotron Radiation in Grenoble (France).

References

- Roldán MV, de Oña P, Castro Y, Durán A, Faccendini P, Lagier C, Grau R, Pellegri NS (2014) Photocatalytic and biocidal activities of novel coating systems of mesoporous and dense TiO₂-anatase containing silver nanoparticles. *Mater Sci Eng C* 43:630–640
- Girginov Ch, Stefchev P, Vitanov P, Hr Dikov (2012) Silver doped TiO₂ photocatalyst for methyl orange degradation. *J Eng Sci Technol Rev* 5:14–17
- Radzig M, Nadtochenko V, Koksharova O, Kiwi J, Lipasova V, Khmel I (2013) Antibacterial effects of silver nanoparticles on gram-negative bacteria: influence on the growth and biofilms formation, mechanisms of action. *Colloids Surf B* 102:300–306
- Roldán MV, Castro Y, Durán A, Pellegri NS (2015) Enhanced photocatalytic activity of mesoporous SiO₂/TiO₂ sol–gel coatings doped with Ag nanoparticles. *J Solgel Sci Technol* 76:180–194
- Suárez S, Coronado JM, Portela R, Martín JC, Yates M, Avila P, Sánchez B (2008) On the preparation of TiO₂-sepiolite hybrid materials for the photocatalytic degradation of TCE: influence of TiO₂ distribution in the mineralization. *Environ Sci Eng* 42:5892–5896
- Hewer TLR, Suárez S, Coronado JM, Portela R, Ávila P, Sánchez B (2009) Hybrid photocatalysts for the degradation of TCE in air. *Catal Today* 143:302–308
- Sakatani Y, Grosso D, Nicole L, Boissière C, de AA Soler-Illia GJ, Sánchez C (2006) Optimised photocatalytic activity of grid-like mesoporous TiO₂ films: effect of crystallinity, pore size distribution, and pore accessibility. *J Mater Chem* 16:77–82
- Arconada N, Castro Y, Durán A, Héquet V (2011) Photocatalytic oxidation of methyl ethyl ketones over sol–gel mesoporous and meso-structured TiO₂ films obtained by EISA method. *Appl Catal B* 107:52–58
- Arconada N, Castro Y, Durán A (2010) Photocatalytic properties in aqueous solution of porous TiO₂-anatase films prepared by sol–gel process. *Appl Catal A* 385:101–107
- Dvoranová D, Brezová V, Mazúr M, Malati MA (2002) Investigations of metal-doped titanium dioxide photocatalysts. *Appl Catal B* 37:91–105
- Zaleska A (2008) Doped-TiO₂: a review. *Recent Pat Eng* 2:157–164
- Akpan UG, Hameed BH (2011) Enhancement of the photocatalytic activity of TiO₂ by doping it with calcium ions. *J Colloid Interface Sci* 357:168–178
- Zhu J, Deng Z, Chen F (2006) Hydrothermal doping method for preparation of Cr³⁺-TiO₂ photocatalysts with concentration gradient distribution of Cr³⁺. *Appl Catal B* 62:329–335
- Khan MR, Chuan TW, Yousuf A, Chowdhury MNK, Kui Cheng C (2015) Schottky barrier and surface plasmonic resonance phenomena towards the photocatalytic reaction: study of their mechanisms to enhance photocatalytic activity. *Catal Sci Technol* 5:2522–2531

15. Žabova H, Sobek J, Církva V, Šolcova O, Kment Š, Hájek M (2009) Efficient preparation of nanocrystalline anatase TiO₂ and V/TiO₂ thin layers using microwave drying and/or microwave calcination technique. *J Solid State Chem* 182:3387–3392
16. Yang Y, Wang H, Li X, Wang C (2009) Electrospun mesoporous W⁶⁺-doped TiO₂ thin films for efficient visible-light photocatalysis. *Mater Lett* 63:331–333
17. Rampaul A, Parkin IP, ÓNeill SA, Desouza J, Mills A, Elliott N (2003) Titania and tungsten doped titania thin films on glass; active photocatalysts. *Polyhedron* 22:35–44
18. Iketani K, De Sun R, Toki M, Hirota K, Yamaguchi O (2004) Sol–gel-derived V_xTi_{1-x}O₂ films and their photocatalytic activities under visible light irradiation Kazuya. *Mater Sci Eng B* 108:187–193
19. Zhao G, Kozuka H, Lin H, Yoko T (1999) Sol–gel preparation of Ti_{1-x}V_xO₂ solid solution film electrodes with conspicuous photoresponse in the visible region. *Thin Solid Films* 339:123–128
20. Al-Salim NI, Bagshaw SA, Bittar A, Kemmitt T, Macquillan AJ, Millsa AM, Ryana MJ (2000) Characterisation and activity of sol–gel-prepared TiO₂ photocatalysts modified with Ca, Sr or Ba ion additives. *J Mater Chem* 10:2358–2363
21. Fu W, Ding S, Wang Y, Wu L, Zhang D, Pan Z, Wang R, Zhang Z, Qiu S (2014) F, Ca co-doped TiO₂ nanocrystals with enhanced photocatalytic activity. *Dalton Trans* 43:16160–16163
22. Li Y, Peng S, Jiang F, Lu G, Li S (2007) Effect of doping TiO₂ with alkaline-earth metal on its photocatalytic activity. *J Serch Chem Soc* 72:393–402
23. Kiriakidou F, Kondarides DI, Verykios XE (1999) The effect of operational parameters and TiO₂-doping on the photocatalytic degradation of azo-dyes. *Catal Today* 54:119–130
24. Herman GS, Gao Y, Tran TT, Osterwalder J (2000) X-ray photoelectron diffraction study of an anatase thin film: TiO₂(001). *Surf Sci* 447:201–211
25. Guglielmi M, Brusatin G, Tombolan N (1993) Ion migration in thin sol-gel glass coatings. *Riv Staz Sper Vetro Sup* 23:495–498
26. Boissiere C, Grosso D, Lepotter S, Nicole L, Brunet AB, Sánchez C (2005) Porosity and mechanical properties of mesoporous thin films assessed by environmental ellipsometric porosimetry. *Langmuir* 21:12362–12371
27. Wang Y, Zhang R, Li J, Li L, Lin S (2014) First-principles study on transition metal-doped anatase TiO₂. *Nanoscale Res Lett* 9:46–53
28. Fortes LM, Gonçalves MC, Almeida RM, Castro Y, Durán A (2013) Nanostructured glass coatings for solar control with photocatalytic properties. *J Non-Cryst Solids* 377:250–253
29. Rosario AV, Christinelli WA, Barreto RN, Pereira EC (2012) Investigation of photocatalytic activity of metal-doped TiO₂ nanoparticles prepared by Pechini method. *J Solgel Sci Technol* 64:734–742
30. Wang W, Tao J, Wang T, Wang L (2007) Photocatalytic activity of porous TiO₂ films prepared by anodic oxidation. *Rare Met* 26:136–141
31. Kment S, Gregora I, Kmentová H, Novatná P, Hubicka Z, Krýsa J, Sajdl P, Dejneka A, Brunclíková M, Jastrabík L, Hrabovský M (2012) Raman spectroscopy of dip-coated and spin-coated sol-gel TiO₂ thin films on different types of glass substrate. *J Solgel Sci Technol* 63:294–306
32. Pillai SC, Periyat P, George R, McCormack DE, Seery MK, Hayden H, Colreavy J, Corr D, Hinder SJ (2007) Synthesis of high-temperature stable anatase TiO₂ photocatalyst. *J Phys Chem C* 111:1605–1611
33. Pal M, Pal U, García JM, Pérez-Rodríguez F (2012) Effects of crystallization and dopant concentration on the emission behavior of TiO₂: Eu nanophosphors. *Nanoscale Res Lett* 7:1–12
34. Yuan Z, Zahng J, Li B, Li J (2007) Effect of metal ion dopants on photochemical properties of anatase TiO₂ films synthesized by a modified sol–gel method. *Thin Solid Films* 515:7091–7095
35. Rashed MN, El-Amin AA (2007) Photocatalytic degradation of methyl orange in aqueous TiO₂ under different solar irradiation sources. *Int J Phys Sci* 2:73–81
36. Sakkas VA, Arabatzis IM, Konstantinou IK, Dimou AD, Albanis TA, Falaras P (2004) Metolachlor photocatalytic degradation using TiO₂ photocatalysts. *Appl Catal B* 49:195–205
37. Chen Y, Dionysiou DD (2008) Bimodal mesoporous TiO₂-P25 composite thick films with high photocatalytic activity and improved structural integrity. *Appl Catal B* 80:147–155
38. Liu S, Min Z, Hu D, Liu Y (2014) Synthesis of calcium doped TiO₂ nanomaterials and their visible light degradation property. In: International conference on material and environmental engineering, pp 43–47
39. Long R, English NJ (2011) Electronic structure of cation-codoped TiO₂ for visible-light photocatalyst applications from hybrid density functional theory calculations. *Appl Phys Lett* 98:142103–142105